Electronic structure and optical properties of binary skutterudite antimonides

Kenji Koga,[1] Koji Akai,[2] Kazunori Oshiro,[1] and Mitsuru Matsuura[1]
[1]*Department of Advanced Materials Science and Engineering, Yamaguchi University, Ube 755-8611, Japan*
[2]*Media and Information Technology Center, Yamaguchi University, Ube 755-8611, Japan*
(Received 8 September 2004; revised manuscript received 15 December 2004; published 27 April 2005)

The electronic structure near the Fermi level of binary skutterudite antimonides and optical properties are studied by the *ab initio* density functional calculation method. Lattice parameters of their compounds are determined by the calculation of the total energy by taking into account the spin-orbit interaction. The calculated band structure shows that lattice parameters strongly affect the band gap and the ordering of electronic states at Γ. $CoSb_3$ is a narrow gap semiconductor with the band gap $E_g=118$ meV. Both $RhSb_3$ and $IrSb_3$ are zero-gap semiconductors, where in $RhSb_3$ a conduction band and a valence band overlap slightly near Γ. Band structures near the gap on binary skutterudite antimonides can be represented by the four band model consisting of the two-band nonparabolic Kane model plus two parabolic bands. By using the band model the thermoelectric power for $CoSb_3$ is calculated. The obtained electronic structure and the wave function are used to calculate and discuss interband optical absorption spectra and the x-ray absorption and emission near edge structure spectra. The calculated x-ray absorption (emission) near edge structure spectra are in good agreement with recent experimental data. Also the valence band density of states is shown to describe the experimental x-ray photoelectron spectra well.

DOI: 10.1103/PhysRevB.71.155119 PACS number(s): 71.20.Nr, 72.20.Pa, 71.15.Nc, 72.15.Jf

I. INTRODUCTION

Research of good thermoelectric materials has been done for a few decades. As these materials are used at various temperature ranges from low to high temperatures, it is necessary to find materials that have large thermoelectric figure of merit $ZT=T\alpha^2\sigma/(\kappa_e+\kappa_l)$ by covering a wide temperature range, where α is a thermoelectric power, σ is an electric conductivity, κ_e and κ_l are an electronic part and a lattice part of thermal conductivities, respectively. In past research several state-of-the-art thermoelectric materials were discovered. For example, one of the well known thermoelectric materials Bi_2Te_3 shows large Z near room temperatures, and PbTe is a good thermoelectric material in a middle temperature region. But it is desirable to find higher ZT materials for cooling devices and energy generating devices. Recently to make a breakthrough for high performance thermoelectric materials, various new type materials are investigated; complex crystal structure systems,[1] strong correlation system as Kondo insulators,[2–4] layered structure materials and mesoscopic structure systems like superlattices.[5,6]

The difficulty in the realization of a high performance thermoelectric material is that it has contradictory conditions; large α, large σ, and low κ. In a simple metal, σ is large, but α is small, and κ_e is large. On the other hand, in an insulator, α is large, but σ is low, and κ_l is large. Thus most candidates of high performance thermoelectric materials are semiconductors. In general semiconductors show large α because of an energy gap at the Fermi level, and with increasing carrier density α decreases exponentially, while σ increases from zero. Thus the power factor $P(=\alpha^2\sigma)$ has a maximum at a certain value of the carrier density and it is necessary to control the carrier density and other physical parameters to realize a large value of P. Recently a concept of "a phonon glass and an electron crystal" (PGEC) is introduced by Slack to realize high performance thermoelectric materials.[7] Skutterudites have obtained much attention for the point of view of PGEC. One of the typical skutterudite compounds $CoSb_3$ have large P in a temperature region 600–800 K and are expected to work as the thermoelectric devices for power generation.[8]

Skutterudite compounds have a complex crystal structure including 32 atoms in a conventional unit cell. Nonetheless electronic structures of many skutterudite compounds have been calculated, as the crystal structure is cubic-based and does not have ambiguity for atomic sites.[9–18] Singh and Pickett calculated the band structure of $CoSb_3$, $CoAs_3$, and $IrSb_3$ using a full potential linear augmented plane wave (FLAPW) method and pointed out that $CoSb_3$ is a direct gap semiconductor with 50 meV and $CoAs_3$ and $IrSb_3$ are gapless semiconductors in which the valence band touches the conduction bands at Γ.[12] The valence band which is singlet just below the Fermi level is proportional to k in the wide k-space region centered at Γ. Sofo and Mahan also calculated the band structure of $CoSb_3$ by a FLAPW method.[13] They optimized the lattice constant and atomic positions of Sb by minimizing the total energy, and showed that the band gap was 170 meV, which is about three times larger than the result of Singh-Pickett. They also pointed out that the k-linear valence band can be described by the Kane's nonparabolic band model.[13] In these previous calculations the spin-orbit (SO) interaction has been neglected except $IrSb_3$, because the effect to the overall band structure is small.

Our group also calculated the electronic structure of $CoSb_3$ with the inclusion of the SO interaction and the theoretical determination of the lattice constant and the Sb positions.[14–16] It was shown that the band edge states of

conduction and valence bands can be described by a pair of the Kane's nonparabolic band and two parabolic bands.[14] Also the x-ray spectra and the thermoelectric property were discussed.[15,16] Takegahara and Harima calculated the electronic structure of some binary skutterudite compounds by a FLAPW method, in which the SO interaction was taken into account and experimental lattice parameters were used, and they obtained the following band gap values: 3 meV ($CoSb_3$), 136 meV (IrP_3), 156 meV ($IrAs_3$), 75 meV ($IrSb_3$).[17] The difference in magnitude of the band gap of $CoSb_3$, calculated theoretically, is related to the difference of lattice parameters. This is because the band gap is much too sensitive for the lattice parameter as pointed out by Singh and Pickett. The calculated electronic density of states were compared with experimental results by x-ray photoelectron spectroscopy (XPS) and reasonable agreement has been obtained.[19,20]

In this paper we present the comprehensive study of the electronic structure and optical spectra in skutterudite antimonides, i.e., we calculate the electronic structure and lattice parameters including the SO interaction in skutterudite antimonides to study band structures near the Fermi level which is characterizing the thermoelectric properties. We show that band parameters are obtained by using a simplified nonparabolic and parabolic bands model. Also the calculated energy and wave function are used to discuss the optical spectra. Especially it will be shown that calculated near edge x-ray absorption and emission spectra agree very well with the experiment recently appeared.

II. COMPUTATIONAL DETAILS

Skutterudite structure is a body-centered-cubic (bcc) structure with $Im\bar{3}(T_h^5)$ and has a large void enclosed by transitional metal (TM) atoms (TM: Co, Rh, Ir) and Sb atoms; the conventional unit cell is shown in Fig. 1. Closed circles denote TM atoms that are in 8*c* sites composed of the simple lattice. Open circles denote Sb atoms that are in 24*g* sites and then four Sb atoms constitute an Sb_4 ring in which an Sb-Sb bond adjacent to a void is shorter than another Sb-Sb bond. The 24*g* site is characterized by two parameters u and v, that are expressed by $(0,u,v)$.

The lattice parameters u, v and the lattice constant a are determined by minimizing the total energy. In the calculation the FLAPW method with the generalized gradient approximation (GGA) is used.[21] The electronic structure calculation is carried out by using the WIEN2K package.[22] The SO interaction for valence electrons is dealt with a second order variational method and core states are computed by using Dirac equations numerically. An exchange-correlation energy is given by the expression of Perdew, Burke, and Ernzerhof with the GGA.[23] The cutoff to the order of spherical harmonics that are a basis of a wave function in an atomic sphere is taken as $L<10$, a cutoff energy of plane waves which are used in the interstitial region is 16.7 Ry. The k-space summation used to calculate the total energy and the Fermi energy is carried out by the tetrahedron method.[24] The k sampling in the irreducible wedge is 24 points in the calculation to obtain lattice parameters, then the irreducible wedge is

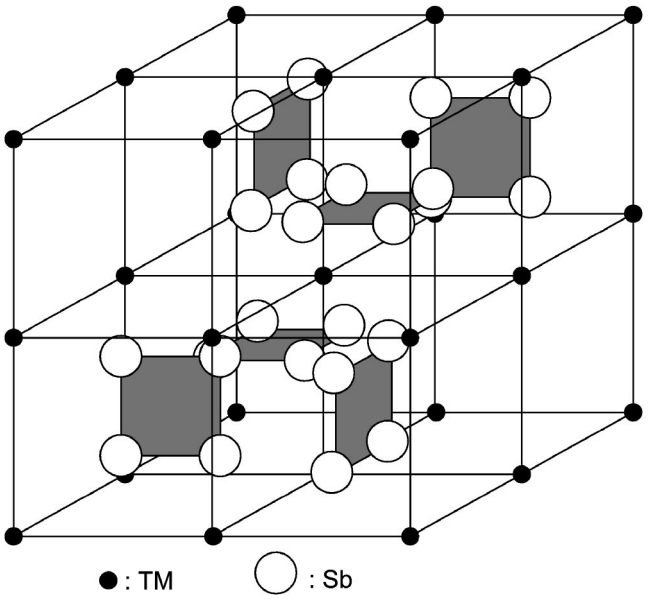

FIG. 1. Conventional unit cell of skutterudite structure. A closed circle denotes a transition metal atom: Co, Rh, Ir and an open circle for antimony.

1/24 of the first Brillouin zone. In the calculation of the density of states of valence electrons and interband optical spectra and the x-ray absorption (emission) near edge structure [XANES (XENES)] spectra, 61 k-sampling points are taken in the wedge and the lattice parameters calculated theoretically are used. A radius of the muffin-tin sphere for each atom is as follows: 2.2 (Co), 2.2 (Rh), 2.2 (Ir), and 2.4 (Sb) in a.u. These muffin-tin spheres are not in contact with each other and size of these spheres is selected within the following condition: lattice parameters are able to adjust without sphere overlapping.

An optical spectroscopy is an effective property to study electronic states of occupied and unoccupied bands and bonding natures. In the present calculation of optical spectra, one body-type treatment is used by the calculated electronic state energy and wave function, then many body-type effects, e.g., effects of final states interaction are not considered. Then the interband optical absorption spectra is given by

$$I_{\mathrm{abs}}^{I}(\omega)=\frac{4\pi\omega}{c}\sum_{n'\mathbf{k}'}^{\mathrm{unocc.}}\sum_{n\mathbf{k}}^{\mathrm{occ.}}\left|\langle n'\mathbf{k}'|\boldsymbol{\varepsilon}\cdot\mathbf{p}|n\mathbf{k}\rangle\right|^2 \times F(\varepsilon_{n'\mathbf{k}'}-\varepsilon_{n\mathbf{k}}-\hbar\omega)\delta_{\mathbf{k}\mathbf{k}'}. \quad (1)$$

Also, the expressions of a XANES and a XENES spectra are given as

$$I_{\mathrm{abs}}^{X}(\omega)=\frac{4\pi\omega}{c}\sum_{n\mathbf{k}}^{\mathrm{unocc.}}\left|\langle n\mathbf{k}|\boldsymbol{\varepsilon}\cdot\mathbf{p}|n_c l_c m_c\rangle\right|^2 F(\varepsilon_{n\mathbf{k}}-\varepsilon_c-\hbar\omega), \quad (2)$$

and

TABLE I. Experimental and theoretical lattice constants, positional parameters, and bulk modulas for binary skutterudite antimonides.

	a (Å)	u	v	B (GPa)
$CoSb_3$				
Expt.	9.0385[a]	0.33537[a]	0.15788[a]	
Theory [this work (GGA)]	9.144	0.3330	0.1592	85
$RhSb_3$				
Expt.	9.2322[b]	0.3420[b]	0.1517[b]	
Theory [this work (GGA)]	9.401	0.3391	0.1550	92
$IrSb_3$				
Expt.	9.2533[b]	0.3407[b]	0.1538[b]	112.4[c]
Theory [this work(GGA)]	9.445	0.3404	0.1537	107

[a]Reference 25.
[b]Reference 26.
[c]Reference 27.

$$I^X_{\mathrm{emi}}(\omega) = 4\pi\hbar\omega^2 \sum_{n\mathbf{k}}^{\mathrm{occ.}} |\langle n_c l_c m_c | \boldsymbol{\varepsilon}\cdot\boldsymbol{p} | n\mathbf{k}\rangle|^2 F(\varepsilon_c - \varepsilon_{n\mathbf{k}} + \hbar\omega), \tag{3}$$

where $\langle\Psi_f|\boldsymbol{\varepsilon}\cdot\boldsymbol{p}|\Psi_i\rangle$ describe the dipole optical transition matrix element between the initial state Ψ_i and the final state Ψ_f and $\boldsymbol{\varepsilon}$ and $\boldsymbol{p}$ are a polarization vector and a dipole operator, respectively. $\varepsilon_{n\mathbf{k}}$ and ε_c are energies of the conduction or the valence electron characterized by n, $\boldsymbol{k}$ and of the core electron with $n_c l_c m_c$, respectively. The spectra are given the broadening factor by the line shape function $F(\omega)$ with a Lorentzian broadening parameter Γ, written as

$$F(\omega) = \frac{1}{2\pi}\frac{\Gamma}{\omega^2 + \Gamma^2}. \tag{4}$$

III. RESULTS AND DISCUSSION

A. Electronic structure and the four-band model

Table I shows calculated lattice parameters, lattice constants, and positional parameters at a Sb atom, and a bulk modulus. Experimentally obtained lattice constants are 9.0385 Å ($CoSb_3$), 9.2320 Å ($RhSb_3$), and 9.2503 Å ($IrSb_3$), respectively.[25,26] The theoretical values are about 1–2% larger than the experimental values. For a bulk modulus the difference between the theoretical value and the experimental one is about 5% in $IrSb_3$.[27] Those theoretical results are in good agreement with the experiments.

Figure 2 shows band structure and total, partial densities of states of skutterudite antimonides. The partial density of states (PDOS) for each element is a sum of a PDOS over all muffin-tin spheres of the same element, respectively. Each orbital component: s, p, d and the sum of them is shown by a thin solid line, a short broken line, a long broken line, and a thick solid line, respectively. The origin of energy is the Fermi energy, i.e., the highest occupied state energy. In Fig. 2 we see that the band edge states, governing the band gap, yield only a very small DOS. In spite of the small density of states these states govern the thermoelectric power as will be seen in a later section. On the other hand the higher and lower electronic states, being distant from band edge, give the large density of states. The energy gap between these states yields the pseudogap and mainly determines optical properties, which will also be shown later. We can see in Fig. 2 that a structure of those DOSs resemble each other. As some authors pointed out,[9,28,29] the leading structure is characterized by the bonding nature of Sb_4 rings and the d orbital of TM (Co, Rh, Ir); the lowest energy part consists of bonding Sb:s orbitals, the second part is bonding Sb:p and TM:d (t_{2g}-like) orbitals and the third part: the conduction bands are nonbonding Sb:p and TM:d (e_g-like) orbitals. The d states of a TM are splitting into t_{2g}-like states and e_g-like states because the TM is at a center of a distorted Sb octahedron. The t_{2g}-like states have a large peak in the second part and the hybridization with Sb:p states is small. DOS of the e_g states are seen at the low energy edge of the third part and the low energy side of the t_{2g} states in Fig. 2. Those two satellite states beside the main d states (t_{2g}-like states) hybridize with Sb:p states strongly. A TM in skutterudite antimonides is nonmagnetic and is a low spin state. Our calculation shows that a TM has about 7 d electrons in a muffin-tin sphere; six electrons are filling t_{2g} states and one electron occupies the hybridized e_g states.

Figure 3 shows the band structure and DOS of skutterudite antimonides for the band edge states. A broken line denotes the energy level of the highest occupied state. It is shown that $CoSb_3$ is a narrow gap semiconductor with a direct gap at Γ. The detailed structure is the following: there is one band near the top of the valence bands and three bands near the bottom of the conduction bands; at Γ there are the singlet occupied state and the doublet and the singlet unoccupied states. The singlet occupied state has $e^u_{1/2}$ symmetry, which is a_u without the SO interaction. The doublet and the singlet unoccupied states have $e^g_{3/2}$ and $e^g_{1/2}$ symmetries, and these states happen to degenerate each other without the SO interaction and have the t_g symmetry. For $RhSb_3$ and $IrSb_3$ they are zero gap semiconductors with slightly overlapping or touching bands near the Γ. As the energy level of the a_u

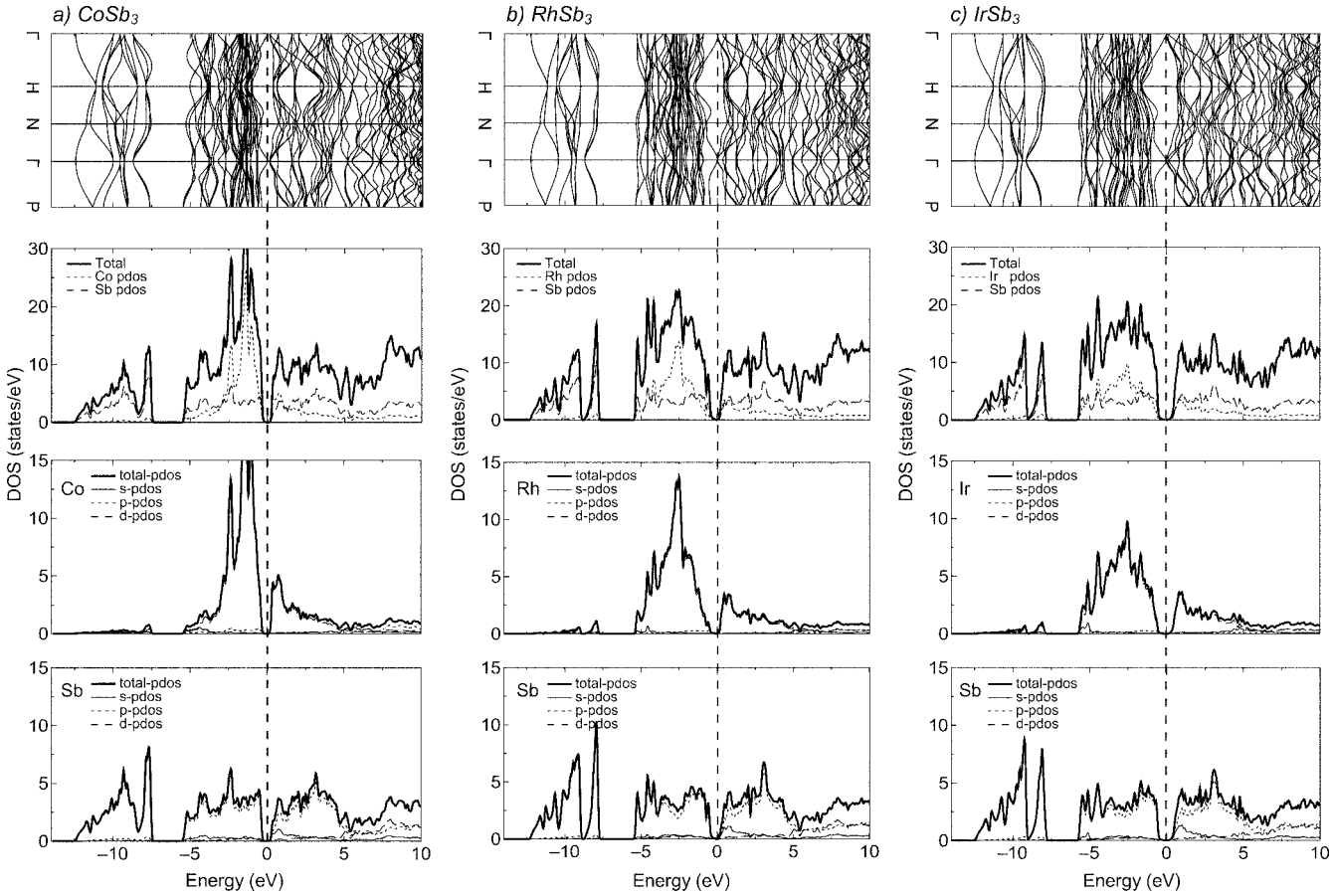

FIG. 2. Band structure, total and partial density of states of skutterudite antimonides: (a) $CoSb_3$, (b) $RhSb_3$, and (c) $IrSb_3$. The origin of energy denotes the top of the occupied states.

state is higher than that of the t_g, the triplet states are occupied partially without the SO interaction. In $RhSb_3$ the ordering of those states is $e^g_{3/2}$, $e^g_{1/2}$, and $e^u_{1/2}$ from the lower energy side. In $IrSb_3$ the situation is more complicated: due to the large SO splitting of the t_g state, the higher energy state $e^u_{1/2}$ comes to be between the $e^g_{3/2}$ and the $e^g_{1/2}$, and thus the ordering is the following: $e^g_{3/2}$, $e^u_{1/2}$, and $e^g_{1/2}$. The $e^u_{1/2}$ state is mainly characterized by p orbitals of Sb and TM elements (Co, Rh, and Ir), then the d-orbital component of the TM element is not included due to the crystal symmetry. The $e^g_{3/2}$ and the $e^g_{1/2}$ states are mainly characterized by the de_g orbital of the TM atom; the distribution of the d orbital is the following: 0.6 ($CoSb_3$), 0.5 ($RhSb_3$), 0.5 ($IrSb_3$).

The SO splitting energy between $e^g_{3/2}$ and $e^g_{1/2}$ at Γ is 23 meV ($CoSb_3$), 43 meV ($RhSb_3$), and 142 meV ($IrSb_3$), respectively. It shows that the SO splitting is small in $CoSb_3$ and $RhSb_3$. But the SO interaction is not negligible to discuss transport properties for these materials. Our GGA result indicates the band gap of $CoSb_3$ is 118 meV with the SO interaction. In the case of neglecting the SO interaction the magnitude of the band gap becomes 173 meV together with the relaxation of lattice parameters. This result is similar to the Sofo-Mahan's result which is 170 meV by the GGA without the SO. The band structure of $IrSb_3$ is in accord with the results of Singh and Pickett in a wide energy range. But the detailed structure near the Fermi level is different, e.g., the SO splitting energy for the triplet state is 118 meV, but the Singh-Pickett's one shows it at about 40 meV.[12]

Band edge states of the conduction and valence bands in skutterudite antimonide can be fitted well by the four bands model consisting of the two parabolic bands plus a pair of the nonparabolic Kane band model,[30] given as

$$\varepsilon_{i\mathbf{k}} = \varepsilon_i^0 + \frac{\hbar^2 k^2}{2m_i} \quad (i = 1,2), \tag{5}$$

$$\frac{\hbar^2 k^2}{2m_v} = \varepsilon_k \left(\frac{\varepsilon_k}{\Delta} - 1 \right). \tag{6}$$

Here Δ is the energy difference between the nonparabolic bands at Γ and m_v is the effective mass. m_1 and m_2 are effective mass of the lowest and the second lowest conduction bands, respectively. In Fig. 3 a dotted line denotes the calculated energy by using the four-band model. In Table II band parameters including a band gap $E_g(=\varepsilon_i^0)$ and a SO splitting energy Δ_{SO} at the triplet states on $CoSb_3$, $RhSb_3$, and $IrSb_3$ are summarized.

B. Thermoelectric power

The thermoelectric power α for p-type $CoSb_3$ has been calculated by Singh-Pickett and Sofo-Mahan with single-

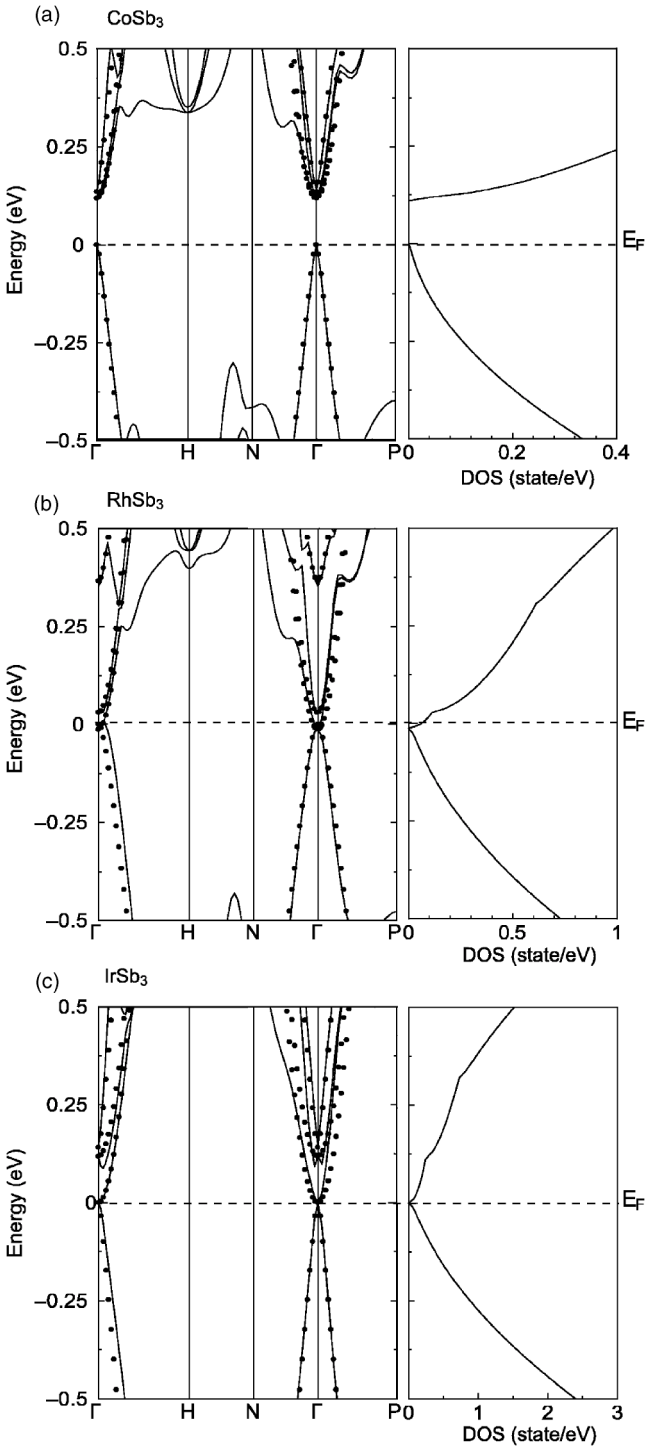

FIG. 3. Band structure and density of states of band edge states in skutterudite antimonides: (a) $CoSb_3$, (b) $RhSb_3$, and (c) $IrSb_3$. Dotted lines in the band structure denote the dispersion calculated by the band model which consists of a pair of the nonparabolic bands and two parabolic bands. Broken lines denote the top of the occupied states.

valence band models, and they demonstrated a temperature dependence below room temperatures.[12,13] By neglecting energy dependence for the carrier relaxation time, α is given as

$$\alpha = \frac{1}{eT}\frac{\sum_{n\mathbf{k}}\left(\frac{\partial f(\varepsilon_{n\mathbf{k}})}{\partial \varepsilon_{n\mathbf{k}}}\right)\boldsymbol{v}_{n\mathbf{k}}^2(\varepsilon_{n\mathbf{k}}-\mu)}{\sum_{n\mathbf{k}}\left(\frac{\partial f(\varepsilon_{n\mathbf{k}})}{\partial \varepsilon_{n\mathbf{k}}}\right)\boldsymbol{v}_{n\mathbf{k}}^2}, \tag{7}$$

where $\boldsymbol{v}_{n\mathbf{k}}=\partial\varepsilon_{n\mathbf{k}}/\partial\hbar\boldsymbol{k}$ and $f(\varepsilon)$ is the Fermi distribution function. Then α is obtained by only the band structure properties. The present calculation is performed with the four-band model under the assumption of the finite concentration of holes, whose value is chosen so that calculation of the thermoelectric power reproduces the experimental value at 100 K. Figure 4 shows the result of temperature dependence for α by using the present four-band model with $E_g=118$ meV. The figure includes also the results of the single-valence band models by Singh-Pickett and Sofo-Mahan. The single valence band models yield the monotonous increase in the thermoelectric power with increasing temperatures. However at higher temperatures the consideration of the conduction band, such as in the four-band model, becomes important. This is because the system becomes in the intrinsic region, i.e., electron excitation from the valence band to the conduction band becomes effective and this causes the cancellation of the electron and hole contributions to the thermoelectric power. The starting of the intrinsic region depends on the band gap E_g. It is well known that the density functional method yields the smaller band gap in many cases. Thus we have performed another calculation with the larger band gap $E_g=148$ meV by shifting the conduction bands. The result, yielding better agreement with the experiment, is also shown in Fig. 4. The experimental data shows a bending near 170 K whose behavior can be described by the four-band model.[31] The theory seems to overestimate the cancellation effects in α at higher temperatures. The calculation can be improved by taking account of (1) impurity levels and (2) scattering mechanisms for carriers which brings the energy dependence to the relaxation time. These effects should be studied in the future.

C. Optical properties

1. Interband optical absorption spectra

In this section we discuss theoretically calculated interband optical absorption spectra on skutterudite antimonides. The interband absorption spectra are shown in Fig. 5 that are computed by substituting the calculated electron energy and the wave functions into (1). In these figures the calculated interband joint density of states (JDOS) are also shown to clarify the effect of symmetric selection properties of the dipole optical transition matrix elements. As seen in Fig. 5, the optical spectra have the similar energy dependence with the corresponding joint density of states. But for $RhSb_3$ and $IrSb_3$ there is the difference for spectral shape between the optical spectra and JDOS around 2.5 eV. The dominant component of the absorption spectra, if the dipole optical transition matrix element is taken into account, are caused by the transition from the *d* component to the *p* component in Rh(Ir) and the *p* component to the *s* component in Sb, and vice versa. The PDOS of the *d* orbitals has the large peak at

TABLE II. Band parameters: band gap E_g, SO splitting energy of the triplet states Δ_{SO}, energy splitting Δ and band masses m_v in the Kane nonparabolic band model, ε_i^0 and m_i are the energy at Γ and the mass of the ith lowest parabolic conduction band on binary skutterudite antimonides.

	E_g (meV)	Δ_{SO} (meV)	Δ (meV)	m_v/m_0	ε_1^0 (meV)	m_1/m_0	ε_2^0 (meV)	m_2/m_0
$CoSb_3$	118	23	141	0.048	118	0.39	118	0.30
$RhSb_3$	0	43	346	0.15	0	0.34	43	0.34
$IrSb_3$	0	142	142	0.065	0	0.40	118	0.39

−2.5 eV as seen in Fig. 2. On the other hand, the shape of JDOS reflects that of the total DOS which is flatter than the PDOS in the same energy region. The difference between the shape of the PDOS and of the total DOS brings the difference between the optical spectra and the JDOS.

By focusing on the lower energy side in Fig. 5, the edgelike structure is marked by arrows. The energy of the edge is given the pseudogap energy (E_{pg}) for skutterudite semiconductors. As shown in Fig. 2, the true gap energy is much smaller than the edge energy. Since the highest valence band is a single band and proportional to k, the magnitude of JDOS above the band gap is small within the pseudogap region compared with that above the pseudogap as seen in the comparison of Figs. 2 and 3. This is reflected in much smaller interband absorption intensity in the region compared with that above the pseudogap. In the calculation of the optical absorption spectra the value of the broadening parameter Γ is taken as 0.1 eV. Then the Lorentzian tail covers the contribution of the highest valence band in the pseudogap region, and makes the smaller effect of the true band gap disappear. From Figs. 2 and 5 we know the magnitude of E_{pg}=0.7 eV ($CoSb_3$), 0.8 eV ($RhSb_3$), 1.2 eV ($IrSb_3$). Slack *et al.* have measured the reflectivity of $IrSb_3$ and estimated the band gap E_g=1.4 eV, which corresponds to the pseudogap energy. It is in good agreement with the theoretical magnitude. The band structure near the pseudogap is characterized by the splitting between the de_g-like and the dt_{2g}-like orbitals of Co group elements. The higher lying valence band with small dispersion at about −1 eV has dt_{2g}-like character. On the other hand, the lower-lying conduction band at about 0.5 eV is characterized by the de_g-like orbital. In future the interband optical absorption experiment may clarify the pseudogaplike behavior.

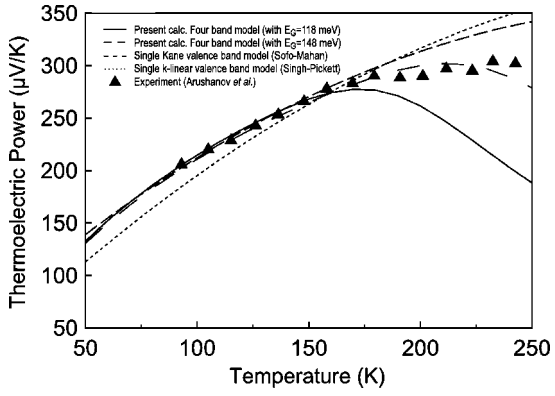

FIG. 4. Thermoelectric power in p-type $CoSb_3$ as a function of temperature. The solid and the broken solid lines are the theoretical results for the four-band model with the band gap E_g=118 meV and 148 meV, respectively. The broken line is the Sofo-Mahan's theoretical one with the single Kane valence band model (Ref. 13). The dotted line is the Singh-Pickett's theoretical one with the single k-linear valence band model (Ref. 12). Closed triangles are the experimental results by Arushanov *et al.* (Ref. 31).

2. X-ray absorption and emission near edge spectra

Calculated x-ray absorption and emission near edge spectra of $IrSb_3$ are shown in Fig. 6 as a typical example. These of the XANES and the XENES spectra are calculated from (2) and (3), respectively. The XENES spectra are shown at the low energy side and the XANES spectra are shown at the high energy side. The resolution of the XANES and XENES seems to vary from the values below 1 eV to a few eV, depending on the related transition and experimental situations. Then we have used three different broadening param-

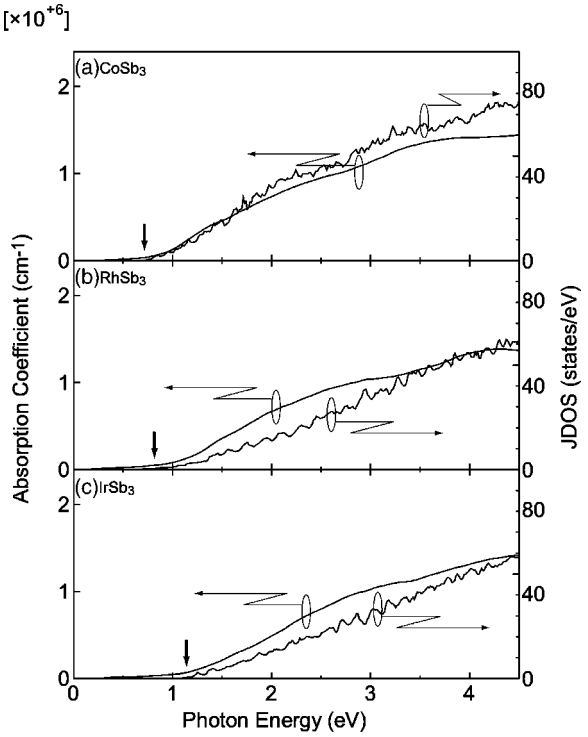

FIG. 5. Theoretically calculated interband optical absorption spectra and joint density of states in skutterudite antimonides: (a) $CoSb_3$, (b) $RhSb_3$, and (c) $IrSb_3$. Broadening parameter Γ is taken to be 0.1 eV.

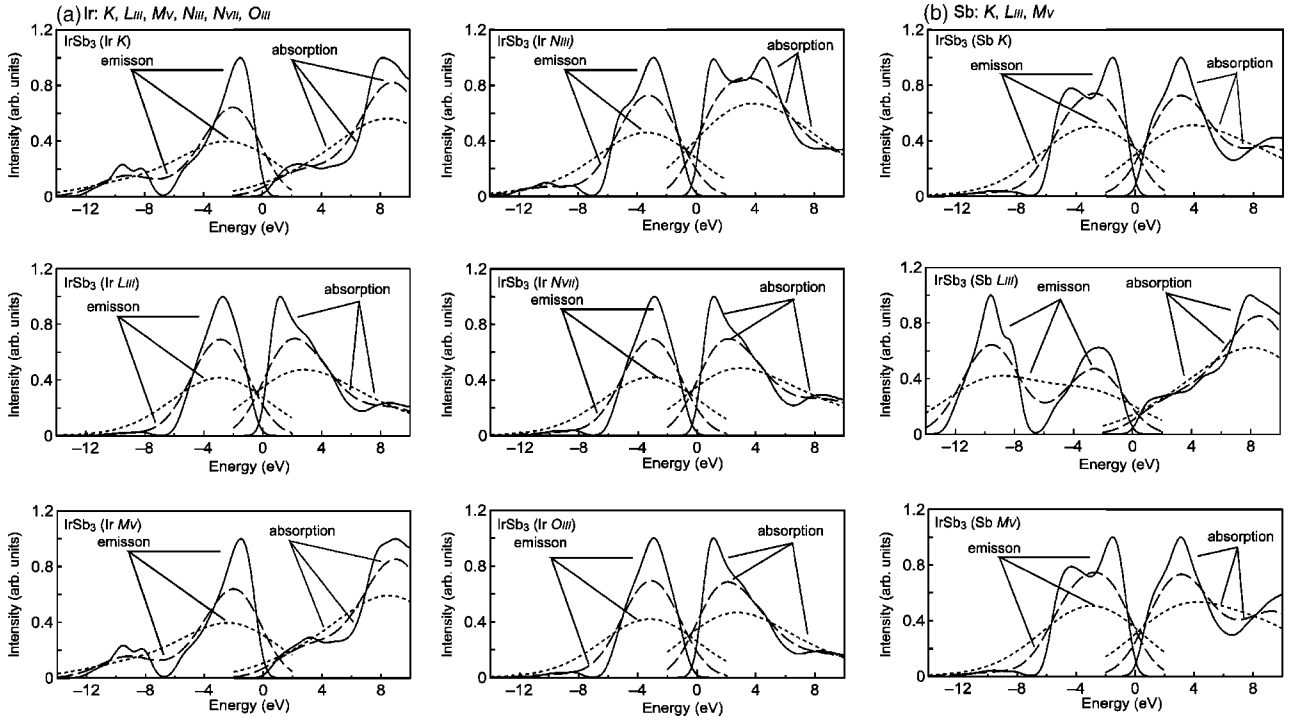

FIG. 6. Theoretical x-ray absorption and emission near edge structure spectra of $IrSb_3$. (a) Ir: K, L_{III}, M_V, N_{III}, N_{VII}, O_{III}. (b) Sb: K, L_{III}, M_V. Broadening parameter Γ is taken to be 0.5 eV, 1.5 eV, and 3 eV: a solid line denotes 0.5 eV, a dashed line denotes 1.5 eV, a dotted line denotes 3 eV, respectively.

eters to demonstrate the broadening parameter dependence on the x-ray spectra; solid lines are $\Gamma=0.5$ eV, broken lines are $\Gamma=1.5$ eV, dotted lines are $\Gamma=3$ eV. The origin of the energy is of the highest occupied state. The core edge structure spectra are originated by the following optical transitions between core states and related character states in valence or conduction states: (a) Ir series: K $1s$ core$\leftrightarrow 6p$ component, L_{III} $2p_{3/2}$ core$\leftrightarrow 6s+5d$ one, M_V $3d_{5/2}$ core$\leftrightarrow 6p$ one, N_{III} $4p_{3/2}$ corelike state$\leftrightarrow 6s+5d$ one, N_{VII} $4f_{7/2}$ corelike state$\leftrightarrow 5d$ one, O_{III} $5p_{3/2}$ corelike state$\leftrightarrow 6s+5d$ one. (b) Sb series: K $1s$ core$\leftrightarrow 5p$ one, L_{III} $2p_{3/2}$ core$\leftrightarrow 5s+4d$ one, M_V $3d_{5/2}$ core$\leftrightarrow 5p$ one.

In the Ir, L_{III} edge spectra s and d components originated from an Ir atom in valence or conduction states are included. In Ir, L_{III} and O_{III}, the main contribution is brought by the $5d$ component from the Ir atom. For the spectra in Ir, N_{VII} reflect only the $5d$ component and the spectra in those cases are much similar to this case. This proportion between the contribution of the $5d$ component and of the $6s$ component reflects in that of partial DOS seen in Fig. 2(c). Contrary to those cases, for the spectral shapes of Ir, N_{III} is different than that of N_{VII}. The difference is caused by the contribution of the $6s$ component. Since in the N_{III} case the magnitude of the dipole element between $4p$ corelike orbitals and $6s$ component is about 4 times larger than that with $5d$ component, the emission and the absorption spectra reflecting in the $6s$ component appear at -5 eV (emission) and 5 eV (absorption) clearly. In Sb both the emission and absorption spectra have two peaks, the lower energy side peak is brought from s component, and another peak is brought from the d component.

It is noted that other core edge structure spectra can be seen from the nine figures in Fig. 6: for example Ir L_I spectra ($2s$ core$\leftrightarrow 6p$ component) is almost the same as Ir K spectra ($1s$ core$\leftrightarrow 6p$ component). We have also calculated x-ray spectra of $CoSb_3$ and $RhSb_3$. The calculated spectra for K, L_{III}, M_V core states are almost the same as to those of $IrSb_3$. Thus Fig. 6 can be used for the study of the XANES and XENES spectra in all skutterudite antimonides.

Figure 7 shows the comparison of the experimental and theoretical XANES and XENES spectra and related partial DOSs of $CoSb_3$ and $RhSb_3$; (a) XANES spectra from Co $K(1s\rightarrow 4p$ component), Sb $L_I(2s\rightarrow 5p$ component), Sb $L_{II}(2p_{1/2}\rightarrow 5s,4d$ components) with a Lorentzian broadening 1.7 eV, (b) XENES spectra to Co $L_{III}(4s,3d$ components$\rightarrow 2p_{3/2})$ with 1.7 eV. For comparison purposes we have also shown the total DOSs of the valence or the conduction band. A solid line is a theoretically calculated spectrum, a dashed-dotted line is an experimental one, and a dotted line is a partial DOS.[32,33]

The calculated energies for these core states are as follows: $E(\mathrm{Co}:K)-E_F=-7.5840$ keV, $E(\mathrm{Co}:L_{III})-E_F=0.7573$ keV, $E(\mathrm{Sb}:L_I)-E_F=-4.6026$ keV, $E(\mathrm{Sb}:L_{II})-E_F=-4.3055$ keV on $CoSb_3$. In Fig. 7 the core state energy is shifted toward the low energy side to reproduce experimental results, i.e., the energy shift $\Delta\hbar\omega_{\mathrm{shift}}=123.3$ eV(Co:K), 20.4 eV(Co:L_{III}), 94.9 eV(Sb:L_I), 75.2 eV(Sb:L_{II}) on $CoSb_3$.

The calculated absorption spectral shapes agree well with the experimental results. The calculated emission spectra are also good agreement with the experimental spectra, though spectral shapes of some shoulders and tails are slightly dif-

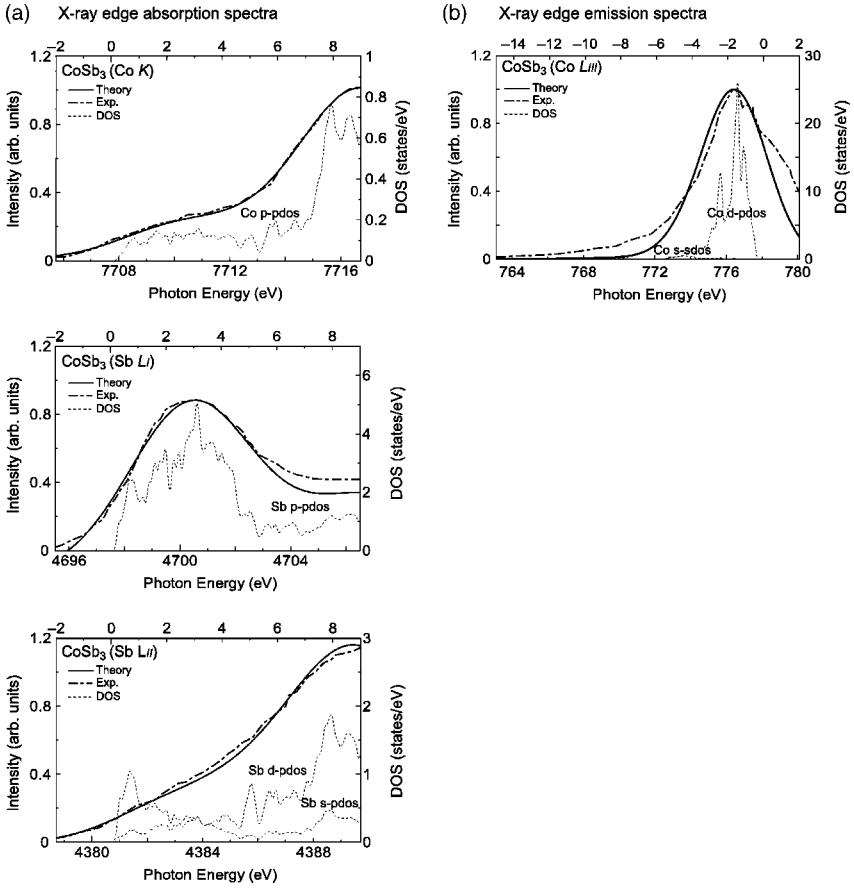

FIG. 7. Comparison of experimental and theoretical x-ray absorption and emission near edge structure spectra and total and partial DOSs with corresponding atomic-orbital character of $CoSb_3$. (a) Absorption spectra from Co-K, Sb-L_I, Sb-L_{II} core states on $CoSb_3$. (b) Emission spectra to a Co-L_{III} core state on $CoSb_3$. A solid line is the theoretical calculation, a dashed-dotted line is the experimental result, and dotted lines are partial DOSs, respectively. In theoretical calculation the broadening parameter Γ is taken to be 1.7 eV.

ferent. As seen in Fig. 7 the shapes of the x-ray edge spectra reflect the corresponding partial DOS's rather than the total DOS's. This is due to the selection rule in the optical transition matrix elements.

3. X-ray photoelectron spectra

We discuss the experimental results of XPS,[20,33] whose valence band spectra can be compared with the valence band density of states. The results of the comparison are shown in Fig. 8. There we have shown the total density of states of valence bands broadened by the Gaussian broadening $w = 0.7$ eV for $CoSb_3$ and $RhSb_3$, together with dominant partial densities of states without broadening. The agreement is good. From the comparison between Figs. 7 and 8 it is seen clearly that the XPS reflects the total density of states, while the x-ray edge emission spectra reflects the related angular component of partial density of states.

IV. CONCLUSION

The electronic structure of skutterudite antimonides $CoSb_3$, $RhSb_3$, and $IrSb_3$ was calculated by the FLAPW method based on the density functional theory with GGA. In the calculation the spin-orbit interaction was included. For lattice parameters, the lattice constant a and the position parameter of Sb u and v were determined by the present computational method. The magnitude of calculated lattice constants agrees well with that of the experiment, though they are slightly longer than the experimental ones. Our calculation shows that $CoSb_3$ is a narrow gap semiconductor with 118 meV; $IrSb_3$ and $RhSb_3$ are zero gap semiconductors. In $RhSb_3$ the conduction band and the valence band overlap slightly at the Γ point. The overlapping is caused by the SO

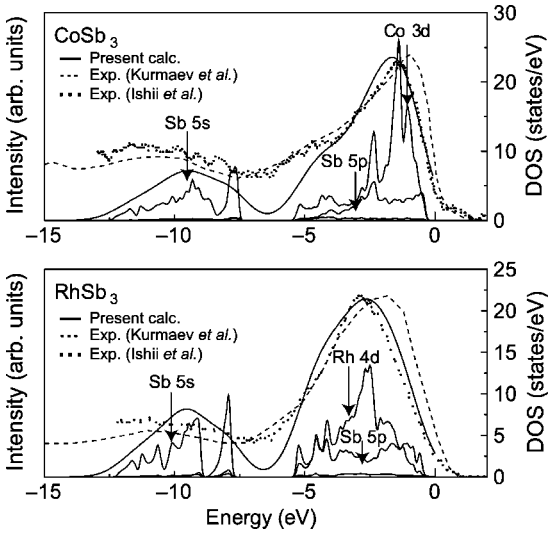

FIG. 8. Comparison of valence band density of states and x-ray photoelectron spectra of $CoSb_3$ and $RhSb_3$. The total density of valence-band states is broadened by the broadening parameter $w = 0.7$ eV for $CoSb_3$ and $RhSb_3$. The dominant partial densities of states are also shown without broadening.

splitting. Band edge states are expressed very well by the four-band model: two free-electron-type conduction bands and a pair of the Kane-type nonparabolic conduction and valence bands. This four-band model is able to reproduce thermoelectric power in $CoSb_3$. The XANES and XENES spectra are calculated and discussed. The good agreement between the calculated and the experimental x-ray spectra is held, especially for XANES in about 10 eV over the Fermi level. Also a calculated valence band density of states is found to reproduce the experimental XPS well. It is noted that inclusion of the spin-orbit interaction affects much of the band edge states and the thermoelectric power, but affects little on the pseudogap states and the optical XANES and XENES spectra.

ACKNOWLEDGMENTS

This work was partly supported by YU-VBL (Yamaguchi University–Venture Business Laboratory).

[1] T. Caillat, S. Chung, J.-P. Fleurial, G. J. Snyder, and A. Borshchevsky, in *Proceedings of the XVII International Conference on Thermoelectrics*, 1998 (unpublished), p. 298.
[2] G. D. Mahan, Phys. Rev. B **56**, 11833 (1997); in *Solid State Physics*, edited by F. Seitz and D. Turnbull (Academic, New York, 1998), Vol. 51.
[3] W. Mao and K. S. Bedell, Phys. Rev. B **59**, R15590 (1999).
[4] K. Fess, W. Kaefer. Ch. Thurner, K. Friemeit, Ch. Kloc, and E. Bucher, J. Appl. Phys. **83**, 2568 (1998).
[5] I. Terasaki, Y. Sasago, and K. Uchinokura, Phys. Rev. B **56**, R12685 (1997).
[6] L. D. Hicks and M. S. Dresselhaus, Phys. Rev. B **47**, 12727 (1993); L. D. Hicks and M. S. Dresselhaus, *ibid.* **47**, 16631 (1993).
[7] G. A. Slack, in *CRC Handbook of Thermoelectrics*, edited by D. M. Rowe (Chemical Rubber, Boca Raton, FL, 1995).
[8] T. Caillat, A. Borshchevsky, and J.-P. Fleurial, J. Appl. Phys. **80**, 4442 (1996).
[9] M. Llunell, P. Alemany, S. Alvarez, V. P. Zhukov, and A. Vernes, Phys. Rev. B **53**, 10605 (1996).
[10] J. L. Feldman and D. J. Singh, Phys. Rev. B **53**, 6273 (1996).
[11] M. Fornari and D. J. Singh, Phys. Rev. B **59**, 9722 (1999).
[12] D. J. Singh and W. E. Pickett, Phys. Rev. B **50**, 11235 (1994).
[13] J. O. Sofo and G. D. Mahan, Phys. Rev. B **58**, 15620 (1999).
[14] K. Akai, K. Oshiro, and M. Matsuura, in *Proceedings of the 18th International Conference on Thermoelectrics, Baltimore, MD, 1999* (IEEE, New York, 1999), p. 444.
[15] K. Koga, K. Akai, K. Oshiro, and M. Matsuura, in *Proceedings of the 20th International Conference on Thermoelectrics, Beijing, 2001* (IEEE, New York, 2001), p. 105.
[16] K. Koga, K. Akai, K. Oshiro, and M. Matsuura, in *Thermoelectric Materials 2001–Research and Applications*, edited by G. S. Nolas, D. C. Johnson, and D. G. Mandrus, MRS Symposia Proceedings No. 691 (Materials Research Society, Pittsburgh, 2001), p. 399.
[17] K. Takegahara and H. Harima, Physica B **328**, 74 (2003).
[18] K. T. Wojciechowski, J. Tobola, and J. Leszczyński, J. Alloys Compd. **361**, 19 (2003).
[19] H. Anno, K. Matsubara, T. Caillat, and J.-P. Fleurial, Phys. Rev. B **62**, 10737 (2000).
[20] H. Ishii, K. Okazaki, A. Fujimori, Y. Nagamoto, T. Koyanagi, and J. O. Sofo, J. Phys. Soc. Jpn. **71**, 2271 (2002).
[21] D. J. Singh, *Planewaves, Pseudopotentials and the LAPW Methods* (Kluwer Academic, Boston, 1994).
[22] P. Blaha, K. Schwarz, G. K. H. Madsen, D. Kvasnicka, and J. Luitz, *An Augmented Plane Wave Plus Local Orbitals Program for Calculating Crystal Properties* (Vienna University of Technology, Austria, 2001), ISBN 3-950131-1-2.
[23] J. P. Perdew, K. Burke, and M. Ernzerhof, Phys. Rev. Lett. **77**, 3865 (1996).
[24] P. E. Blochl, O. Jepsen, and O. K. Andersen, Phys. Rev. B **49**, 16223 (1994).
[25] T. Schmidt, G. Gliche, and H. D. Lutz, Acta Crystallogr., Sect. C: Cryst. Struct. Commun. **43**, 1678 (1987).
[26] A. Kjekshus and T. Rakke, Acta Chem. Scand., Ser. A **28**, 99 (1978).
[27] G. A. Slack and V. G. Tsoukala, J. Appl. Phys. **76**, 1665 (1994).
[28] D. Jung, M.-H. Whangbo, and S. Alvarez, Inorg. Chem. **29**, 2251 (1990).
[29] V. P. Zhukov, Fiz. Tverd. Tela (St. Petersburg) **38**, 166 (1996) [Phys. Solid State **38**, 90 (1996)].
[30] E. O. Kane, in *Semiconductors and Semimetals*, edited by R. K. Willardson and A. C. Beer (Academic, New York, 1966), Vol. 1, Chap. 3.
[31] E. Arushanov, K. Fess, W. Kaefer, Ch. Kloc, and E. Bucher, Phys. Rev. B **56**, 1911 (1997).
[32] I. Lefebvre-Devos, M. Lassalle, X. Wallart, J. Olivier-Fourcade, L. Monconduit, and J. C. Jumas, Phys. Rev. B **63**, 125110 (2001).
[33] E. Z. Kurmaev, A. Moewes, I. R. Shein, L. D. Finkelstein, A. L. Ivanovskii, and H. Anno, J. Phys.: Condens. Matter **16**, 979 (2004).